

Comprehensive numerical study of the Adelaide Jet in Hot-Coflow burner by means of RANS and detailed chemistry

Zhiyi Li^{a,*}, Alberto Cuoci^b, Amsini Sadiki^c, Alessandro Parente^{a,**}

^a*Université Libre de Bruxelles, Aero-Thermo-Mechanics Department, Belgium*

^b*Politecnico di Milano, Department of Chemistry, Materials, and Chemical Engineering "G. Natta", Italy*

^c*Technische Universität Darmstadt, Institute of Energy and Powerplant technology, Germany*

Abstract

The present paper shows an in-depth numerical characterisation of the Jet in Hot Co-flow (JHC) configuration using the Reynolds Averaged Navier-Stokes (RANS) modelling with detailed chemistry. The JHC burner emulates the MILD combustion by means of a hot and diluted co-flow and high speed injection. The current investigation focuses on the effect of turbulent combustion models, turbulence model parameters, boundary conditions, multi-component molecular diffusion and kinetic mechanisms on the results. Results show that the approaches used to model the reaction fine structures, namely as Perfectly Stirred Reactors (PSR) or Plug Flow Reactors (PFR), do not have a major impact on the results. Similarly, increasing the complexity of the kinetic mechanism does not lead to major improvements on the numerical predictions. On the other hand, the inclusion of multi-component molecular diffusion helps increasing the prediction accuracy. Three different Eddy Dissipation Concept (EDC) model formulations are compared, showing their interaction with the choice of the $C_{1\epsilon}$ constant in the $k - \epsilon$ turbulence model. Finally, two approaches are benchmarked for turbulence-chemistry interactions, the EDC model and the Partially Stirred Reactor (PaSR) model.

Keywords: Eddy Dissipation Concept, Jet in Hot Co-flow burner,

*Zhiyi.Li@ulb.ac.be

**Alessandro.Parente@ulb.ac.be

Abbreviations

JHC	Jet in Hot Co-flow
RANS	Reynolds Averaged Navier-Stokes
MILD	Moderate or Intense Low oxygen Dilution
PSR	Perfectly Stirred Reactor
PFR	Plug Flow Reactor
EDC	Eddy Dissipation Concept
LES	Large Eddy Simulation
RSM	Reynolds Stress Model
PaSR	Partially Stirred Reactor
FVM	Finite Volume Method
GCI	Grid Convergence Index
CPU	Central Processing Unit
TVD	Total Variation Diminishing
LUD	Linear Upwind
CDS	Central Differencing Scheme
ODE	Ordinary Differential Equation
ISAT	In-situ Adaptive Tabulation

1. Introduction

Facing the challenges of energy shortage and limited fossil fuel resources, as well as the increasing air pollution problems, the development of fuel flexible, efficient and environmentally friendly combustion technologies has become urgent. Some new combustion technologies appeared during the last few decades. Among those, the Moderate or Intense Low oxygen Dilution (MILD) combustion [1, 2] has drawn increasing attention recently. MILD combustion is characterised by diluted reactants, non-visible or audible flames and uniform distributed temperatures [3, 4, 5]. As a result, complete combustion can be assured and the formation of pollutants such as CO, NO_x [6, 7] and soot are strongly reduced [8, 9]. More recently, there are also some investigations focused on the applicability of MILD combustion to oxy-fuel conditions [10, 11], in order to further reduce the pollutants.

According to Li et al.[12], high temperature pre-heating of combustion air and the high-speed injection of fuel are the main requirements to achieve MILD combustion condition. Based on these requirements, model flames like the Adelaide Jet in Hot Co-flow (JHC) burner [13] and Delft JHC burner [14, 15] were built to emulate MILD condition. The Adelaide JHC burner has a central high speed jet and secondary burners providing hot exhaust products mixing with air. Dally et al. [13] have carried out experiments on this burner with central jet fuel of CH₄ and H₂, in equal proportions on a molar basis. Different oxygen levels (9%, 6% and 3%) are fixed in the hot co-flow. Medwell et al. [16] used laser diagnostic to reveal the distribution of hydroxyl radical (OH), formaldehyde (H₂CO), and temperature under the influences of hydrogen addition. They also found out that the weak to strong transition of OH and the appearance of H₂CO are the evidences for the occurrence of pre-ignition in the apparent lifted region of ethylene flames [17].

In addition to experimental investigations, increasing attention has been paid to the numerical modelling of MILD combustion. Most of the numerical investigations were carried out using Reynolds Averaged Navier-Stokes (RANS) simulation or Large Eddy Simulation (LES). The LES approach is able to capture more details of the flame, while RANS is still important in the industrial context or for the early stage academic research because of its reduced computational cost. Due to the strong mixing and

the reduced temperature levels in MILD combustion, a stronger competition between chemistry reaction and fluid dynamics exists in this regime. This leads to a system characterised by a relatively low Damköhler number ($Da = \text{turbulence_time_scale}/\text{chemical_time_scale}$). As a result, the interactions between the fluid dynamics and chemical reaction become more important. Thus, they need to be carefully considered in the modelling process. In terms of chemical kinetics, global mechanisms are not sufficient to capture the main features of MILD combustion [18]. Using a turbulent combustion model with the possibility of implementing detailed mechanism plays a vital role therefore. Different approaches were evaluated by Shabanian et al. [19], Christo et al. [20], Parente et al. [21, 22], Fortunato et al. [23] and Galletti et al. [24] employing Reynolds Averaged Navier-Stokes (RANS) simulation. In these approaches, the authors showed that the Eddy Dissipation Concept (EDC) [25] model can better handle the strong interactions between turbulence and chemistry with respect to the classic flamelet approaches. The EDC model splits every computational cell into two regions: the fine structures, where reactions take place, and the surrounding fluid mixture. In the original EDC formulation, the fine structures are modelled as Perfectly Stirred Reactors (PSR). However, they are also modelled as Plug Flow Reactors (PFR) in some software packages for numerical reasons. To the author’s knowledge, up to now there is no study showing the impact of such a choice on the results. Beside chemistry, turbulence model also influences the accuracy of prediction. Frassoldati et al. [26] compared the performances of several RANS models, the standard $k - \epsilon$ model, modified $k - \epsilon$ model ($C_{1\epsilon}$ adjusted from 1.44 to 1.60), and Reynolds Stress Model (RSM). The modified $k - \epsilon$ model was found to better reproduce experimental data, as also indicated by Christo et al. [20]. Moreover, there exist different formulations of the EDC model [27, 28, 25]. The combination of the $k - \epsilon$ parameters with different EDC formulations has not been studied yet. This will be discussed in the present paper. Beside the EDC model, other combustion models such as the Partially Stirred Reactor (PaSR) [29] combustion model and closures based on the Perfectly Stirred Reactor (PSR) [30] have been proposed to simulate MILD combustion. In the present paper, the PaSR model is compared to the EDC model.

Apart from the turbulence and chemistry models, there are other modelling aspects that require careful evaluation. The strong mixing and uniform temperature field result in a lower reaction rate in MILD combustion. Therefore, molecular diffusion effects are enhanced [20], especially when H_2

is present in the fuel, due to its significant molecular diffusion coefficient. Christo et al. [20] and Mardani et al.[31] showed that the numerical predictions for the JHC burner could be improved by including laminar diffusion in the solver. Besides, the EDC model was found to perform reasonably well for an oxygen content in the co-flow of 9% and 6%, while an over-prediction of the temperature level downstream of the jet outlet was observed for the 3% case [20]. According to Parente et al. [32], the over-prediction can be alleviated by adjusting the EDC parameters of C_γ and C_τ . They derived the dependence of the C_γ and C_τ parameters on the Kolmogorov Damköhler number, Da_η and turbulent Reynolds Number, Re_T . With the proposed formulations for Da_η and Re_T in MILD combustion, C_γ and C_τ were adjusted accordingly [32].

Up to now, quite a few sensitivity analyses have been conducted on the JHC burner, to investigate the effect of different modelling choices, including the turbulent and chemistry models, model parameters, co-flow oxygen levels and molecular diffusion. However, a comprehensive sensitivity study of the JHC burner has not been yet carried out. In the current paper, the influences of turbulence model parameters, combustion models (closures based on PSR and PFR, as in EDC or PaSR), molecular diffusion, uniform and non-uniform boundary conditions as well as the kinetic mechanisms will all be presented and discussed. The purpose of this paper is to provide a deep and comprehensive study on the sensitivity of model predictions in MILD combustion regime and to extend it to a wider range of modelling choices.

2. Experimental Basis

The validation test case used in the present work is taken from the Adelaide JHC burner[13]. They include different fuel types, various jet Reynolds numbers and co-flow oxygen levels. The Adelaide JHC burner has an insulated and cooled central jet with the inner diameter of 4.25 *mm*. The central fuel jet provides an equi-molar mixture of CH₄ and H₂. A secondary burner mounted upstream of the exit plane has the inner diameter of 82 *mm*. It provides the hot combustion products. The combustion products are mixed with air and nitrogen, thus oxygen level can be controlled with the amount of nitrogen added. The oxygen level is adjusted to 3%, 6% and 9%. The wind tunnel on which the burner is mounted has the cross section of 254 *mm* × 254 *mm*. In Fig. 1, a 2D sketch of the domain investigated in the numerical simulation is presented. The gas temperature and velocity profiles

of the central jet, annulus and wind tunnel can be found in Table 1. In the present study, the condition corresponding to a Reynolds number of 10000 and and co-flow oxygen content of 3% is investigated.

[Figure 1 about here.]

[Table 1 about here.]

The single-point Raman-Rayleigh-laser-induced fluorescence technique was applied in the experimental measurement. The mean and variance profiles of temperature and mass fractions of species (CH_4 , H_2 , H_2O , CO_2 , N_2 , O_2 , NO , CO , and OH) along the centerline as well as on the radial position of 30/60/120/200 mm are available. More details about the Adelaide JHC burner experiment carried out by Dally et al. can be found in [13].

3. Mathematical Models

The Reynolds Average Navier-Stokes (RANS) based simulations are carried out on the Adelaide JHC MILD burner. Turbulence chemistry interactions are handled with EDC (Eddy Dissipation Concept) and with PaSR (Partially Stirred Reactor) models. Detailed chemistry can be applied with both models. The OpenFOAM[®][33] Finite Volume Method (FVM) based, open-source CFD software is used for all simulations. The model equations solved by the code are shown in the following sections.

3.1. Turbulence Model

In RANS simulations, the density-based Favre-averaged (denoted with $\tilde{\cdot}$) governing equations of mass, momentum and energy are solved [34] :

$$\frac{\partial \bar{\rho}}{\partial t} + \frac{\partial}{\partial x_j} (\bar{\rho} \tilde{u}_j) = 0, \quad (1)$$

$$\frac{\partial}{\partial t} (\bar{\rho} \tilde{u}_i) + \frac{\partial}{\partial x_j} (\bar{\rho} \tilde{u}_i \tilde{u}_j) = -\frac{\partial \bar{p}}{\partial x_i} + \frac{\partial}{\partial x_j} \left(\bar{\tau}_{ij} - \widetilde{\bar{\rho} u_i'' u_j''} \right), \quad (2)$$

$$\frac{\partial}{\partial t} (\bar{\rho} \tilde{h}) + \frac{\partial}{\partial x_j} (\bar{\rho} \tilde{h} \tilde{u}_j) = \frac{\partial}{\partial x_j} \left(\bar{\rho} \alpha \frac{\partial \tilde{h}}{\partial x_j} - \widetilde{\bar{\rho} u_j'' h''} \right) - \frac{\partial}{\partial x_j} (\bar{q}_{rj}) + \bar{S}_{hc}. \quad (3)$$

In Eqn. 1 - 3, ρ , \mathbf{u} , p represent the density, velocity and pressure respectively; h is the enthalpy; α is the thermal diffusivity. The term \mathbf{q}_r denotes the radiative heat loss and S_{hc} is the source term coming from combustion process. The turbulent heat flux is modelled as:

$$-\overline{\rho u_j'' h''} \approx \frac{\mu_t}{Pr_t} \frac{\partial \tilde{h}}{\partial x_j}, \quad (4)$$

where Pr_t is the turbulent Prandtl number, set to 0.85 in the present work [35].

In combustion processes, multiple species are involved. The Favre averaged transport equation of species Y_s reads:

$$\frac{\partial}{\partial t} (\overline{\rho \tilde{Y}_s}) + \frac{\partial}{\partial x_j} (\overline{\rho \tilde{Y}_s \tilde{u}_j}) = \frac{\partial}{\partial x_j} \left(\left(\overline{\rho} D_{m,s} + \frac{\mu_t}{Sc_t} \right) \frac{\partial \tilde{Y}_s}{\partial x_j} \right) + \tilde{\omega}_s, \quad (5)$$

where Sc_t is the turbulent Schmidt number and $D_{m,s}$ is the molecular diffusion coefficient for species s in the mixture. In the current paper, a Sc_t value of 0.7 is used [36].

Previous works on the JHC burner ([20, 26]) have shown that the modified $k - \epsilon$ model, based on the adjustment of the $C_{1\epsilon}$ constant in the turbulent dissipation transport equation, is well suited for this configuration. The $k - \epsilon$ model is based on solving the transport equations of turbulence kinetic energy \tilde{k} and the dissipation rate $\tilde{\epsilon}$ of the turbulence kinetic energy [34]:

$$\frac{\partial}{\partial t} (\overline{\rho \tilde{k}}) + \frac{\partial}{\partial x_j} (\overline{\rho \tilde{k} \tilde{u}_j}) = \frac{\partial}{\partial x_j} \left(\left(\mu + \frac{\mu_t}{\sigma_k} \right) \frac{\partial \tilde{k}}{\partial x_j} \right) + G_k - \overline{\rho \tilde{\epsilon}}, \quad (6)$$

$$\frac{\partial}{\partial t} (\overline{\rho \tilde{\epsilon}}) + \frac{\partial}{\partial x_j} (\overline{\rho \tilde{\epsilon} \tilde{u}_j}) = \frac{\partial}{\partial x_j} \left(\left(\mu + \frac{\mu_t}{\sigma_\epsilon} \right) \frac{\partial \tilde{\epsilon}}{\partial x_j} \right) + C_{1\epsilon} \overline{\rho \frac{\tilde{\epsilon}}{k}} G_k - C_{\epsilon 2} \overline{\rho \frac{\tilde{\epsilon}^2}{k}}, \quad (7)$$

in which G_k is the turbulence kinetic energy production rate. The model constants in Eqn. 6 and Eqn. 7 are C_μ , $C_{1\epsilon}$, $C_{\epsilon 2}$, σ_k and σ_ϵ . The $C_{1\epsilon}$ constant is increased from 1.44 to 1.60 in the modified $k - \epsilon$ model. The other constants do not change [37].

3.2. Combustion Models

3.2.1. EDC Model

The Eddy Dissipation Concept (EDC) combustion model assumes that combustion takes place in the fine structures where the dissipation of the flow turbulence kinetic energy occurs. In the original model by Magnussen [27], the fine structures are modelled as Perfectly Stirred Reactors (PSR). However, some software packages (for example, ANSYS Fluent [38]) treat them as Plug Flow Reactors (PFR), mainly for numerical reasons. EDC is based on a cascade model providing the mass fraction of the fine structures, γ_λ , and the mean residence time of the fluid within the fine structures τ^* , as a function of the flow characteristic scales:

$$\gamma_\lambda = C_\gamma \left(\frac{\nu \tilde{\epsilon}}{\tilde{k}^2} \right)^{\frac{1}{4}}, \quad (8)$$

$$\tau^* = C_\tau \left(\frac{\nu}{\tilde{\epsilon}} \right)^{\frac{1}{2}}. \quad (9)$$

In Eqn. 8 and Eqn. 9, ν is the kinematic viscosity, $C_\gamma = 2.1377$ and $C_\tau = 0.4083$ are model constants in the EDC model [25]. The mean reaction rate (source term in the species transport equation) is expressed as [28]:

$$\bar{\omega}_s = -\frac{\bar{\rho} \gamma_\lambda^2}{\tau^* (1 - \gamma_\lambda^3)} \left(\tilde{Y}_s - Y_s^* \right). \quad (10)$$

The term \tilde{Y}_s in Eqn. 10 denotes the mean mass fraction of the species s between the fine structures and the surrounding fluid and Y_s^* is the mass fraction of species s in the fine structures. The mean mass fraction \tilde{Y}_s can be expressed as a function of Y_s^* and Y_s^0 (mass fraction of species s in the surrounding fluids):

$$\tilde{Y}_s = \gamma_\lambda^3 Y_s^* + (1 - \gamma_\lambda^3) Y_s^0. \quad (11)$$

The expressions of the species mean reaction rate and mean mass fraction in Eqn. 10 and Eqn. 11 were proposed by Gran et al. in 1996 [28], thus it will be referenced as 'EDC1996' in the rest of the paper.

In the earlier version of the EDC model, proposed originally by Magnussen in 1981 [27], the mean reaction rate of species s is given by

$$\bar{\dot{\omega}}_s = -\frac{\bar{\rho}\gamma_\lambda^3}{\tau^*(1-\gamma_\lambda^3)} \left(\tilde{Y}_s - Y_s^* \right). \quad (12)$$

This formulation will be referred as 'EDC1981'. Later in 2005, Magnussen modified the model [25], expressing $\bar{\dot{\omega}}_s$ as:

$$\bar{\dot{\omega}}_s = -\frac{\bar{\rho}\gamma_\lambda^2}{\tau^*(1-\gamma_\lambda^2)} \left(\tilde{Y}_s - Y_s^* \right), \quad (13)$$

and mean mass fraction \tilde{Y}_s as

$$\tilde{Y}_s = \gamma_\lambda^2 Y_s^* + (1 - \gamma_\lambda^2) Y_s^0. \quad (14)$$

This version of EDC model will be denoted as 'EDC2005'.

In all three formulations, the mean mass fraction \tilde{Y}_s is obtained by solving the species transport equation. The mass fraction of each species inside the fine structure Y_s^* is computed with the finite-rate chemistry approach.

Finite-rate Chemistry Approach

The mass fraction Y_s^* of species s inside the fine structures is evaluated by modelling them to a Perfectly Stirred Reactor (PSR) [28]:

$$\frac{\dot{\omega}_s^*}{\rho^*} = \frac{1}{\tau^*} (Y_s^* - Y_0), \quad (15)$$

in which $\dot{\omega}_s^*$ is the formation rate of species s . Alternatively, the fine structures can be modelled as Plug Flow Reactors (PFR), evolving in a characteristic time equal to τ^* :

$$\frac{dY_s}{dt} = \frac{\dot{\omega}_s}{\rho}. \quad (16)$$

The final integration over $\frac{dY_s}{dt}$ is Y_s^* . The term $\dot{\omega}_s$ is the instantaneous formation rate of species s coming from a detailed kinetic mechanism. In the present study, the KEE (17 species, 58 reactions) [39], GRI3.0 (53 species, 325 reactions) [40], San-Diego (50 species, 247 reactions) [41] and POLIMI_C1C3HT (107 species, 2642 reactions) [42] mechanisms are used. N-containing species are only included in the mechanisms for a selected number of simulations, as they do not effect the main combustion process.

Limitation of Fine Structure Fraction

In the EDC model, the chemical reaction process and mixing are interconnected. This mixing process time scale τ_{mix} should be larger or equal to the fine structures residence time scale τ^* . Defining R as the ratio [43]:

$$R = \frac{\tau^*}{\tau_{mix}} = \frac{\gamma_\lambda^2}{1 - \gamma_\lambda^3}, \quad (17)$$

one can find the limit value for γ_λ . The ratio R and γ_λ limits for the various EDC formulations can be found in Table 2.

[Table 2 about here.]

3.2.2. The Partially Stirred Reactor model

The Partially Stirred Reactor (PaSR) concept, originally proposed by Chomiak [29], assumes that every computational cell can be separated into two zones. All the reactions take place in one zone, while no reactions occur in the other zone [44]. Thus, the chemical reaction rate for the species s can be expressed with:

$$\bar{\omega}_s = \kappa \dot{\omega}_s^*(\tilde{\mathbf{Y}}, \tilde{T}). \quad (18)$$

In the equation above, $\dot{\omega}_s^*(\tilde{\mathbf{Y}}, \tilde{T})$ is the formation rate of species s based on the mean species concentration in the cell. The term κ is the factor that provides the *partially stirred* condition. It is formulated as:

$$\kappa = \frac{\tau_c}{\tau_c + \tau_{mix}}, \quad (19)$$

where τ_c is the chemical time scale, estimated by rate of formation of each species and taking the highest limiting value as the characteristic one. The term τ_{mix} is the mixing time scale. In the present work, the mixing time scale is taken as the geometric mean of the integral and Kolmogorov mixing time scales:

$$\tau_{mix} = \left(\frac{\tilde{k}}{\tilde{\epsilon}} \cdot \sqrt{\frac{\nu}{\tilde{\epsilon}}} \right)^{\frac{1}{2}}. \quad (20)$$

The inherent idea behind PaSR model has similarities with the EDC model. But the mathematical formulations are different. This makes it interesting to compare the simulation results from these two combustion models.

3.3. Numerical Settings

In this section, the numerical settings for the JHC simulations are presented in detail.

A 2-dimensional axis-symmetric mesh is used in the simulations. A grid convergence study was carried out to optimise the number of cells. The Grid Convergence Index (GCI) [45] was calculated for different mesh resolutions, as indicated in Table 3 for four mesh resolutions. The medium mesh resolution was chosen, because it provides a reasonable compromise between CPU time requirements and numerical accuracy. The selected mesh has 30150 hexahedral cells and 450 prisms. The burner walls are ignored in the domain. The computation domain starts from the burner exit and extends 1000 *mm* downstream.

[Table 3 about here.]

The second order discretization schemes are applied for the governing equations. An overview of selected numerical schemes can be found in Table 4.

[Table 4 about here.]

Both uniform and non-uniform boundary conditions are used in the simulation for the species mass fractions and temperature. The uniform boundary conditions are obtained from the theoretical data provided by Dally et al. [13], as they are shown in Table 5. The non-uniform ones are obtained from the mean sampled experimental value 4 *mm* downstream of the jet exit. Since no velocity profiles are provided in the experimental data base, uniform inlet velocity is specified based on the Reynolds number.

[Table 5 about here.]

The transient solver `edcPimpleSMOKE` based on the open source software `OpenFOAM`[®] is used. The solver and EDC model implementation come from `edcSMOKE` [46, 47].

A reference case is defined to have a clear understanding of the discrepancies between the different cases in the sensitivity analysis. The numerical settings of the reference case are listed in Table 6. The multi-component molecular diffusion is included because of the existence of Hydrogen in the fuel. Preliminary simulations with both `OpenFOAM`[®] and `ANSYS Fluent`

14.5 [38] solvers were carried out to investigate the influence of radiation effects. The Discrete Ordinates Method (DOM) radiation model in combination with the Weighted Sum of Gray Gases (WSGG) absorption emission model was used. Results showed that the radiation effects have minor impact on the temperature and species mass fraction profiles at the locations where experimental data are available and they can be neglected without loss of accuracy.

[Table 6 about here.]

4. Results and Discussion

In this section, the simulation results compared with the experimental measurements are presented and discussed. Based on the reference case in Table 6, one parameter at time is investigated. The impact of the different parameters on the temperature and species mass fraction profiles represents the focus of this section.

4.1. Turbulence Model Parameters

The impact of various turbulence model parameters on the results was investigated, including the turbulent Schmidt number (Eqn. 5), the turbulent Prandtl number (Eqn. 4) and the $k - \epsilon$ model constant $C_{1\epsilon}$ (Eqn. 7). For brevity, only the influence of $C_{1\epsilon}$ is discussed in this section, while the effect of Sc_t and Pr_t numbers is shown in the supplementary material.

In a round jet flow, Dally et al. [48] confirmed that there is an over-prediction of decay rate and the spreading rate when the standard $C_{1\epsilon}$ constant value [37] is applied in the $k-\epsilon$ model. The authors concluded that $C_{1\epsilon} = 1.60$ helped to improve the prediction of the flow and mixing field. This was confirmed by the other authors ([20, 26]) as well. In this paper, the same conclusion can be made under the condition that the 'EDC1996' version (in Eqn. 10) of the combustion model is used. In Fig. 2, the advantages of setting $C_{1\epsilon} = 1.60$ over $C_{1\epsilon} = 1.44$ are very clear. For the model versions 'EDC1981' and 'EDC2005', the results are discussed in the following subsection.

[Figure 2 about here.]

4.2. Combustion Model Parameters

In this subsection, the effects of the combination of EDC formulations and $C_{1\epsilon}$ value mentioned in Section 4.1 will be further discussed, along with the effect of the EDC model constants and canonical reactors simulating the fine structures.

4.2.1. EDC model formulation

The earliest 'EDC1981' formulation was indicated in Eqn. 12. When it is combined with two different $C_{1\epsilon}$ value, the results shown in Fig. 3 are obtained. Here, the adjusted $C_{1\epsilon}$ constant has the advantages of better predicting the experimental values.

However, the 'EDC2005' model formulation shows different features. In Fig. 4, the case with $C_{1\epsilon} = 1.44$ better predicts the experimental values than that with $C_{1\epsilon} = 1.60$. This indicates the existence of a strong interplay between turbulence and combustion model formulations. In particular, the evaluation of the mean mass fraction using Eqns. 11 and 14 has the strongest impact on the results. If it is assumed that the fine structures are localised in nearly constant energy regions (Eqn. 14), then the most appropriate choice is the use of the standard formulation of the k- ϵ model, as the over-estimation of the jet spread [49] is compensated by a reduced mass exchange between the fine structures and the surroundings. When the round-jet analogy is corrected by a modified $C_{1\epsilon}$ constant, it is clear that the most appropriate assumption for the EDC model is that the mass exchange between the fine structures is volumetric (Eqn. 11).

[Figure 3 about here.]

[Figure 4 about here.]

4.2.2. EDC model constants

From the former results (Fig. 2 - Fig. 4), it is not hard to find out that there is an obvious over-prediction of the peak temperature downstream of the jet, especially at the position of 120 *mm*. This agrees with the outcome from Christo et al. [20]. There are different authors [50, 19, 51, 32] who used the approach of adjusted EDC constants to alleviate the over-predicted temperature peak. Among them, the adjustment proposed by Parente et al. [32] is not simply based on a fitting procedure, but it arises from a phenomenological analysis on the chemical and fluid dynamics scales in MILD combustion.

Therefore, the adjustment of the EDC constants from Parente et al. [32] is adopted here in order to reduce the peak temperature. The model constant C_γ is decreased from 2.1377 to 1.9 and C_τ is increased from 0.4083 to 1.47. This setting is denoted as 'Adjusted-1'. It results in a decreased fine structures mass fraction and increased residence time. The results of the mean temperature values can be found in Fig. 5. The temperature peaks are successfully suppressed by 6.5% and 10.8% at axial positions of 60 and 120 *mm* respectively. However, temperature peak at axial position of 120 *mm* is still over-predicted by 17.9%. In order to further investigate the effect of the model constants, a second set of adjusted values is used, with $C_\gamma = 1.5$ and $C_\tau = 1.47$. It is indicated as 'Adjusted-2'. Compared with the standard values of the parameters, the 'Adjusted-2' constants reduce the temperature peak at 120 *mm* axial location by 17.1%. This has however an effect on the centerline temperature, which is reduced slightly with respect to the experimental values.

The effect of the adjusted EDC parameters on the flow field is also investigated. Because the lack of experimental velocity profile, the mixture fraction profile constructed from the Bilger's definition [39] is shown in Fig. 6. The profiles from three set of parameters (Standard, Adjusted-1 and Adjusted-2) are virtually identical, with very minor differences visible only on the centerline starting from 120 *mm* axial position. This indicates that the modification of the model constants only impacts the species and temperature profile, with a negligible effect on the turbulent mixing field.

Overall, the proposed EDC constants by Parente et al. [32] ('Adjusted-1') help to alleviate the temperature over-prediction at axial locations above 60 *mm* from the burner exit. However, the observed reduction of the temperature peak in the present work is less significant to the one shown by Parente et al. [32], and comparable results can be obtained only using the 'Adjusted-2' settings. This discrepancies can be likely attributed to the different discretization schemes used. Indeed, the present investigation is based on the half second order discretization schemes of Total Variation Diminishing (TVD) on the divergence terms, while the results by Parente et al. [32] were obtained using the fully second order schemes of Linear Upwind (LUD) or Central Differencing Scheme (CDS) on the divergence term.

[Figure 5 about here.]

[Figure 6 about here.]

4.2.3. PSR vs. PFR closures for the fine structures

The Perfectly Stirred Reactor (PSR) is generally used as the canonical reactor to simulate the fine structures in EDC model. Numerically speaking, the use of Plug Flow Reactor (PFR) can help improving the robustness. That's because PFR is described by a set of Ordinary Differential Equations (ODEs) with initial conditions, while a PSR is described by a set of algebraic non-linear equations, whose solution requires an iterative procedure. Moreover, even though the solution of a ODE system is generally more expensive than an algebraic non-linear system, the PFR can be more easily combined with tabulation method like In-situ Adapted Tabulation (ISAT) to increase computational efficiency. The purpose of this subsection is to determine whether PFR can be used instead of PSR without loss of accuracy. The comparison of the results obtained with the two approaches is shown in Fig. 7, Fig. 8 and Fig. 9, for the temperature, H₂O, OH and CO mass fraction profiles, respectively. The mean temperature profiles as well as the mean H₂O mass fraction from the cases with PFR and PFR are very close to each other and virtually identical. The same conclusion holds for other major species. For the minor species, the profiles of CO and OH at axial positions of 30 *mm* and 60 *mm* show close results with PSR and PFR in Fig. 9. Therefore, PFR can be used instead of PSR in EDC model, to simulate the fine structures.

[Figure 7 about here.]

[Figure 8 about here.]

[Figure 9 about here.]

4.2.4. EDC VS. PaSR

In this part, the results from EDC model and the newly implemented PaSR model are benchmarked.

Fig. 10 shows the experimental profiles of temperature as well as the computed ones using EDC and PaSR models at different axial locations and along the centerline. It can be observed that the PaSR model reduced the temperature over-prediction at axial position 60 *mm*. Most importantly, the highly over-predicted 120 *mm* temperature peak is alleviated to a large extent. The similar conclusion can be drawn looking at the CO₂ mass fraction profiles, shown in Fig. 11. In particular, NO emissions are largely over-predicted

(more than two times) using EDC model, as a result of the temperature over-prediction. Conversely, predictions based on the PaSR model are quite accurate, at both 120 *mm* and 200 *mm* axial locations.

[Figure 10 about here.]

[Figure 11 about here.]

[Figure 12 about here.]

4.3. Boundary Conditions

In RANS simulation, uniform inlet boundary values of the species, velocity and temperature are generally used. In the current work, the profiles of species mass fractions and temperature accessible from the experimental data at 4 *mm* from the burner exit are used to simulate non-uniform boundary conditions. Thus, the simulation results with the uniform and non-uniform boundary conditions are compared in Fig. 13, Fig. 14 and Fig. 15, where the mean profiles of temperature, H₂O mass fraction and CO mass fraction are presented, respectively.

[Figure 13 about here.]

[Figure 14 about here.]

[Figure 15 about here.]

In Fig. 13, it can be observed that the non-uniform boundary conditions help to reduce the peak temperature at the different axial positions, and the centerline temperature is also slightly decreased. The differences between using the uniform and non-uniform boundary conditions can be better identified in Fig. 14. In the near centerline regions, the H₂O mass fraction values are not well predicted by the non-uniform boundary conditions, while the values far from the centerline are well predicted. In particular, the use of non-uniform boundary conditions allows to recover the non-zero values of H₂O mass fractions at axial positions corresponding to 30 and 60 *mm*. The over prediction of H₂O mass fraction values at axial position of 120 *mm* and along the centerline is alleviated with non-uniform boundary conditions. However, at 30 and 60 *mm* axial positions, the peak mass fraction is not well predicted, and a general under-prediction can be observed. The obvious

advantage of using the non-uniform boundary conditions is revealed by the analysis of CO profiles in Fig. 15. The experimental data show two peaks for the mean CO mass fraction at different radial positions. When uniform boundary conditions are applied, only one peak appears in the CO mass fraction profiles. The second peak can be recovered by providing non-uniform boundary conditions. In conclusion, the non-uniform boundary conditions help to better predict the jet surrounding regions. Nevertheless, it shows some deficiencies in predicting the major species H_2O in the jet core region.

4.4. Multi-component Molecular Diffusion

Because of the presence of H_2 in the fuel stream, it is necessary to consider the effect of molecular diffusivity of the calculated profiles. The inclusion of multi-component molecular diffusion is carried out following Eqn. 5. Moreover, the transport of enthalpy due to species diffusion is included in the energy equation. The mean temperature profiles with and without multi-component molecular diffusion are shown in Fig. 16. It can be observed that, without molecular diffusion, it is not possible to capture the correct temperature peak at 30 *mm* axial position and along the centerline. The temperature peak without molecular diffusion is 5% lower than the experimental one at axial position of 30 *mm*. A slight temperature over-prediction can be observed using molecular diffusion at 60 and 120 *mm* axial positions. However, this can be suppressed using the adjusted EDC constants C_γ and C_τ , as indicated in Section 4.2.2. Furthermore, as shown in Fig. 17, the inclusion of the multi-component molecular diffusion term helps increasing the accuracy of H_2O predictions near centerline regions. The peak values of H_2O at axial positions of 30 and 60 *mm* are increased by about 13-15% with the inclusion of molecular diffusion.

[Figure 16 about here.]

[Figure 17 about here.]

4.5. Kinetic Mechanisms

In MILD combustion, the use of detailed mechanisms is essential to capture finite rate chemistry effects. The EDC model closure allows to account for detailed chemistry via the canonical reactors used to model the fine structures. In the present work, the KEE, GRI3.0, San-Diego and POLIMI_C1C3HT mechanisms were chosen, as mentioned in Section 3.2.1,

with the objective of determining the degree of complexity required to correctly capture the main features of the combustion regime. The sampled numerical profiles obtained with the mechanisms are compared with experimental data in Fig. 18 and Fig. 19. The main observation is that the results provided by the different mechanisms do not show major differences. The GRI3.0, San-Diego and POLIML_C1C3HT mechanisms correct the slightly over-predicted centerline mean temperature, with respect to the predictions of the KEE mechanism. The same trend can be observed for the major species mass fractions. For other species, minor differences are observed for the OH radical (Fig. 19 top), while the KEE mechanism better captures the CO peak value. On the other hand, the simulation cost of GRI3.0, San-Diego and POLIML_C1C3HT is 3.7, 4.8 times and 14.3 times the cost of KEE, respectively. This makes the usage of large mechanisms not strictly necessary in the current case.

[Figure 18 about here.]

[Figure 19 about here.]

5. Conclusion

In the present work, the Adelaide Jet in Hot Co-flow burner was numerically investigated by means of RANS simulations with detailed kinetic mechanisms. The study focuses on the effect of various parameters on the results, including $k - \epsilon$ model constant, the combustion model formulation (formulation of EDC and PaSR, combustion model constants and choice of the canonical reactors simulating the fine structures), boundary conditions definition, multi-component molecular diffusion and degree of complexity of the kinetic mechanisms.

The main results can be summarised as follows:

- A strong interplay between combustion and turbulence model formulation is found. In particular, the EDC formulations 'EDC1981' and 'EDC1996' result in a better agreement with the experimental data when the $k - \epsilon$ model constant $C_{1\epsilon} = 1.60$. When $C_{1\epsilon} = 1.44$, the 'EDC2005' formulation provides the best results.
- The fine structures can be modelled using PFR equations without loss of accuracy. This helps increasing the robustness of calculation and

offers the potential of a more straightforward coupling with tabulation method like In-situ Adaptive Tabulation (ISAT).

- The use of non-uniform boundary conditions allows improving species predictions, especially away from centerline region.
- Multi-component molecular diffusion is found to play an important role, due to the presence of H_2 in the fuel. This is in agreement with the work carried out by Christo et al. [20] and Mardani et al. [31].
- Minor differences in the predictions are observed between using KEE mechanism and kinetic mechanisms with increasing complexity (GRI3.0, San-Diego and POLIMI_C1C3HT). The use of a more comprehensive mechanism nevertheless improves the prediction of the centerline temperature.
- The over-prediction of the temperature peak at 120 *mm* axial position with EDC model can be alleviated by using modified constants.
- The benchmark between EDC and PaSR models shows that both models are suitable for simulating MILD regimes. Further investigations are needed for the PaSR model, in order to clarify the effect of turbulent and chemical time scale calculations on the predictions.

The developed model is characterised by sufficient complexity to allow its application in presence of gaseous mixtures with various components, including hydrogen. This is a very attractive feature of the approach towards its application to model modern combustion technologies designed to deal with multiple fuels and non-conventional combustion regimes.

6. Acknowledgement

This project has received funding from the European Union’s Horizon 2020 research and innovation program under the Marie Skłodowska-Curie grant agreement No 643134, and from the Fédération Wallonie-Bruxelles, via ‘Les Actions de Recherche Concertée (ARC)’ call for 2014 - 2019, to support fundamental research.

References

- [1] J. A. Wüning, J. G. Wüning, Flameless oxidation to reduce thermal NO-formation, *Progress in Energy and Combustion Science* 23 (1997) 81–94.
- [2] A. Cavaliere, M. de Joannon, MILD combustion, *Progress in Energy and Combustion Science* 30 (2004) 329–366.
- [3] B. B. Dally, E. Riesmeier, N. Peters, Effect of fuel mixture on moderate and intense low oxygen dilution combustion, *Combustion and Flame* 137 (2004) 418–431.
- [4] M. de Joannon, G. Sorrentino, A. Cavaliere, MILD combustion in diffusion-controlled regimes of hot diluted fuel, *Combustion and Flame* 159 (2012) 1832–1839.
- [5] X. Gao, F. Duan, S. C. Lim, M. S. Yip, NO_x formation in hydrogen-methane turbulent diffusion flame under the moderate or intense low-oxygen dilution conditions, *Energy* 59 (2013) 559–569.
- [6] Y. He, C. Zou, Y. Song, Y. Liu, C. Zheng, Numerical study of characteristics on NO formation in methane MILD combustion with simultaneously hot and diluted oxidant and fuel (HDO/HDF), *Energy* 112 (2016) 1024–1035.
- [7] M. Ferrarotti, C. Galletti, A. Parente, L. Tognotti, Development of reduced NO_x models for flameless combustion, in: 18th IFRF Members Conference, 2015.
- [8] G. G. Szegö, B. B. Dally, G. J. Nathan, Scaling of NO_x emissions from a laboratory-scale MILD combustion furnace, *Combustion and Flame* 154 (2008) 281–295.
- [9] A. Mardani, S. Tabejamaat, S. Hassanpour, Numerical study of CO and CO₂ formation in CH₄/H₂ blended flame under MILD condition, *Combustion and Flame* 160 (2013) 1636–1649.
- [10] Y. Liu, S. Chen, S. Liu, Y. Feng, K. Xu, C. Zheng, Methane combustion in various regimes: First and second thermodynamic-law comparison between air-firing and oxyfuel condition, *Energy* 115 (2016) 26–37.

- [11] A. Mardani, A. F. Ghomshi, Numerical study of oxy-fuel MILD (Moderate or intense Low-oxygen Dilution combustion) combustion for CH₄/H₂ fuel, *Energy* 99 (2016) 136–151.
- [12] P. Li, J. Mi, Influence of inlet dilution of reactants on premixed combustion in a recuperative furnace, *Flow Turbulence and Combustion* 87 (2011) 617–638.
- [13] B. B. Dally, A. N. Karpetis, R. S. Barlow, Structure of turbulent non-premixed jet flames in a diluted hot coflow, *Proceedings of the Combustion Institute* 29 (2002) 1147–1154.
- [14] E. Oldenhof, M. J. Tummers, E. van Veen, D. Roekaerts, Ignition kernel formation and lift-off behaviour of Jet-in-Hot-Coflow flames, *Combustion and Flame* 157 (2010) 1167–1178.
- [15] E. Oldenhof, M. J. Tummers, E. H. van Veen, D. J. E. M. Roekaerts, Role of entrainment in the stabilisation region of Jet-in-Hot-Coflow flames, *Combustion and Flame* 158 (8) (2011) 1553–1563.
- [16] P. R. Medwell, B. B. Dally, Effect of fuel composition on jet flames in a heated and diluted oxidant stream, *Combustion and Flame* 159 (2012) 3138–3145.
- [17] P. R. Medwell, P. A. Kalt, B. B. Dally, Imaging of diluted turbulent ethylene flames stabilized on a Jet in Hot Coflow (JHC) burner, *Combustion and Flame* 152 (2007) 100–113.
- [18] A. Parente, J. Sutherland, B. Dally, L. Tognotti, P. Smith, Investigation of the MILD combustion regime via principal component analysis, *Proceedings of the Combustion Institute* 33 (2011) 3333–3341.
- [19] S. R. Shabaniyan, P. R. Medwell, M. Rahimi, A. Frassoldati, A. Cuoci, Kinetic and fluid dynamic modeling of ethylene jet flames in diluted and heated oxidant stream combustion conditions, *Applied Thermal Engineering* 52 (2012) 538–554.
- [20] F. C. Christo, B. B. Dally, Modelling turbulent reacting jets issuing into a hot and diluted coflow, *Combustion and Flame* 142 (2005) 117–129.

- [21] A. Parente, C. Galletti, L. Tognotti, Effect of the combustion model and kinetic mechanism on the MILD combustion in an industrial burner fed with hydrogen enriched fuels, *international journal of hydrogen energy* 33 (2008) 7553–7564.
- [22] A. Parente, C. Galletti, L. Tognotti, A simplified approach for predicting NO formatio in MILD combustion of CH₄/H₂ mixtures, *Proceeding of the Combustion Institute* 33 (2011) 3343–3350.
- [23] V. Fortunato, C. Galletti, L. Tognotti, A. Parente, Influence of modelling and scenario uncertainties on the numerical simulation of a semi-industrial flameless furnace, *Applied Thermal Engineering* 76 (2014) 324–334.
- [24] C. Galletti, A. Parente, L. Tognotti, Numerical and experimental investigation of a mild combustion burner, *Combustion and Flame* 151 (2007) 649–664.
- [25] B. F. Magnussen, The eddy dissipation concept a bridge between science and technology, in: *ECCOMAS Thematic Conference on Computational Combustion*, Lisbon, Portugal, 2005.
- [26] A. Frassoldati, P. Sharma, A. Cuoci, T. Faravelli, E. Ranzi, Kinetic and fluid dynamics modeling of methane/hydrogen jet flames in diluted coflow, *Applied Thermal Engineering* 30 (2009) 376–383.
- [27] B. F. Magnussen, On the structure of turbulence and a generalized eddy dissipation concept for chemical reaction in turbulent flow, in: *19th AIAA Aerospace Science Meeting*, St. Louis, Missouri, USA, 1981.
- [28] I. Gran, B. F. Magnussen, A numerical study of a bluff-body stabilized diffusion flame, part 2: Influence of combustion modelling and finite-rate chemistry, *Combustion Science and Technology* 119 (1-6) (1996) 191–217.
- [29] J. Chomiak, *Combustion: A Study in Theory, Fact and Application*, Abacus Press/Gorden and Breach Science Publishers, 1990.
- [30] F. Wang, P. Li, Z. Mei, J. Z. and Jianchun Mi, Combustion of CH₄ /O₂ /N₂ in a well stirred reactor, *Energy* 72 (2014) 242–253.

- [31] A. Mardani, S. Tabejamaat, M. Ghamari, Numerical study of influence of molecular diffusion in the MILD combustion regime, *Combustion Theory and Modelling* 14 (5) (2010) 747–774.
- [32] A. Parente, M. R. Malik, F. Contino, A. Cuoci, B. B. Dally, Extension of the eddy dissipation concept for turbulence/chemistry interactions to MILD combustion, *Fuel* 163 (2015) 98–111.
- [33] H. G. Weller, G. Tabor, H. Jasak, C. Fureby, A tensorial approach to computational continuum mechanics using object-oriented techniques, *COMPUTERS IN PHYSICS* 12 (6).
- [34] D. A. Lysenko, I. S. Ertesvåg, K. E. Rian, Numerical simulation of non-premixed turbulent combustion using the eddy dissipation concept and comparing with the steady laminar flamelet model, *Flow, Turbulence and Combustion* 53 (2014) 577–605.
- [35] S. Vodret, D. Vitale, D. Maio, G. Caruso, Numerical simulation of turbulent forced convection in liquid metals, *Journal of Physics: Conference Series* 547.
- [36] Y. Tominaga, T. Stathopoulos, Turbulent schmidt numbers for CFD analysis with various types of flowfield, *Atmospheric Environment* 41 (2007) 8091–8099.
- [37] B. E. Launder, D. B. Spalding, The numerical computations of turbulent flows, *Computer Methods in Applied Mechanics and Engineering*.
- [38] ANSYS® Academic Research, Release 14.5.
- [39] R. W. Bilger, S. H. Stårner, R. J. KEE, On reduced mechanisms for methane-air combustion in nonpremixed flames, *Combustion and Flame* 80 (2) (1990) 135–149.
- [40] G. P. Smith, D. M. Golden, M. Frenklach, N. W. Moriarty, B. Eiteneer, M. Goldenberg, C. T. Bowman, R. K. Hanson, S. Song, W. C. Gardiner, Jr., V. V. Lissianski, Z. Qin. [link].
URL http://www.me.berkeley.edu/gri_mech/
- [41] Chemical-kinetic mechanisms for combustion applications.
URL <http://combustion.ucsd.edu>

- [42] E. Ranzi, A. Frassoldati, R. Grana, A. Cuoci, T. Faravelli, A. Kelley, C. Law, Hierarchical and comparative kinetic modeling of laminar flame speeds of hydrocarbon and oxygenated fuels, *Progress in Energy and Combustion Science* 38 (4) (2012) 468–501.
- [43] A. De, E. Oldenhof, P. Sathiah, D. Roekaerts, Numerical simulation of Delft-Jet-in-Hot-Coflow (DJHC) flames using the eddy dissipation concept model for turbulencechemistry interaction, *Flow Turbulence Combustion* 87 (2011) 537–567.
- [44] F. P. Kärrholm, Numerical modelling of diesel spray injection, turbulence interaction and combustion, Ph.D. thesis, Chalmers University of Technology (2008).
- [45] P. Roache, *Fundamentals of Computational Fluid Dynamics*, Hermosa Publishers, 1998.
- [46] [link].
URL <https://github.com/acuoci/edcSMOKE>
- [47] M. R. Malik, Z. Li, A. Cuoci, A. Parente, Edcsmoke: A new combustion solver based on openfoam, in: *Tenth Mediterranean Combustion Symposium*, 2017.
- [48] B. B. Dally, D. F. Fletcher, A. R. Masri, Flow and mixing fields of turbulent bluff-body jets and flames, *Combustion Theory and Modelling* 2 (1998) 193–219.
- [49] S. Pope, *Turbulent Flows*, Cambridge University Press, 2011.
- [50] J. Aminian, C. Galletti, S. Shahhosseini, L. Tognotti, Numerical investigation of a MILD combustion burner: Analysis of mixing field, chemical kinetics and turbulence-chemistry interaction, *Flow, Turbulence and Combustion* 88 (4) (2012) 597–623.
- [51] M. J. Evans, P. R. Medwell, Z. F. Tian, Modelling lifted jet flames in a heated coflow using an optimised eddy dissipation concept model, *Combustion Science and Technology* 187 (7) (2015) 1093–1109.

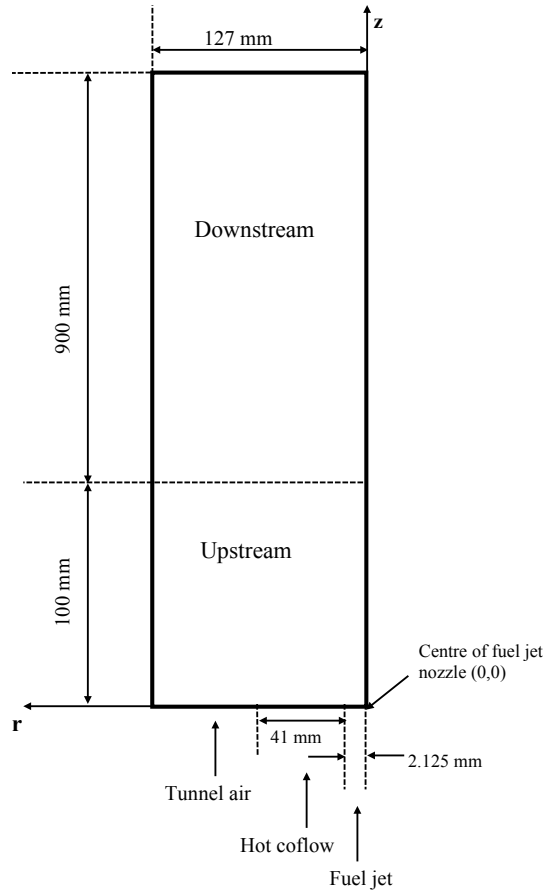


Figure 1: 2D sketch of the Adelaide Jet in Hot Co-flow burner (adapted from Ferrarotti et al. [7]).

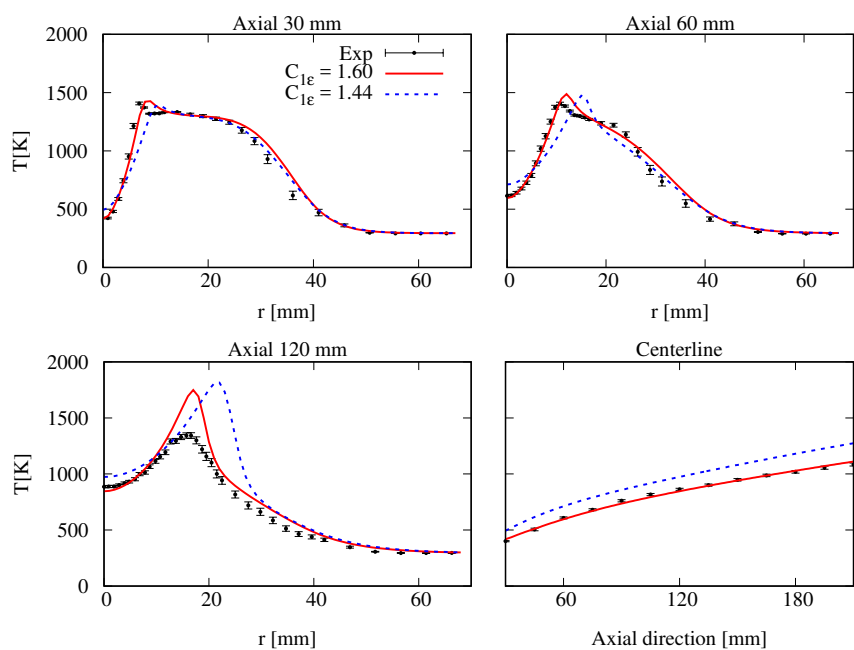


Figure 2: Effects of k - ϵ model parameter $C_{1\epsilon}$ on predicted mean temperature profiles at several axial locations in radial direction and along the centerline (EDC model version: 'EDC1996').

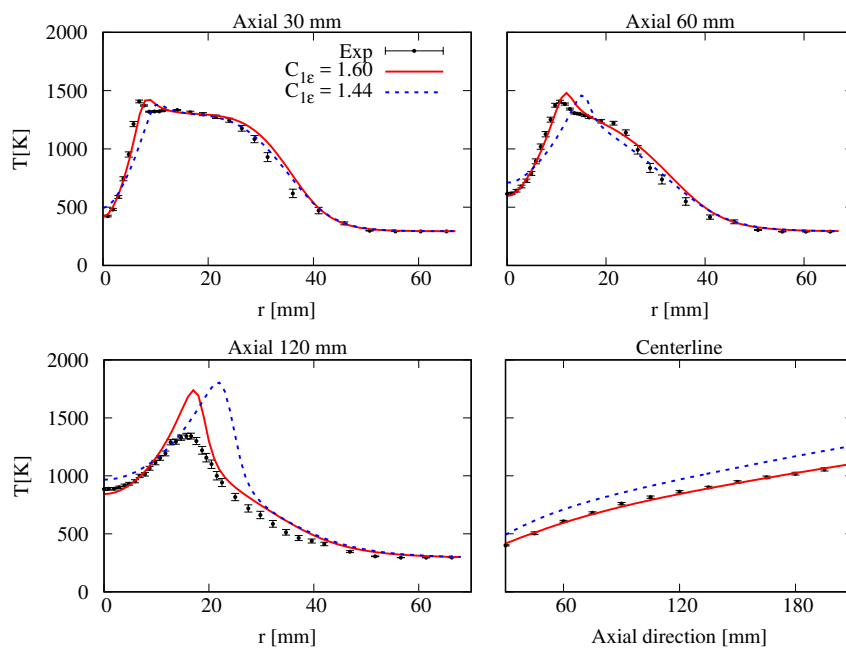


Figure 3: Effects of k - ϵ model parameter $C_{1\epsilon}$ on predicted mean temperature profiles at several axial locations in radial direction and along the centerline (EDC model version: 'EDC1981').

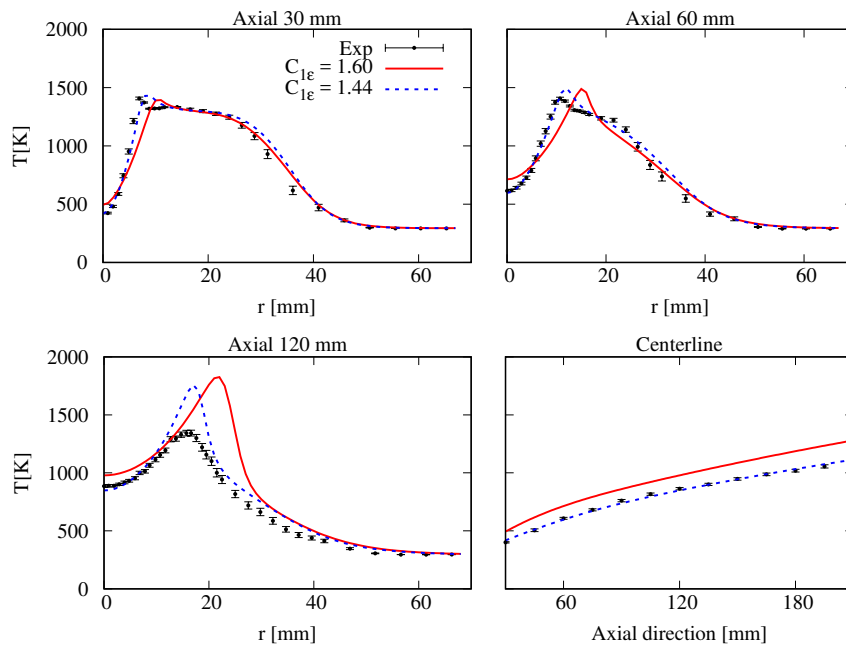


Figure 4: Effects of k - ϵ model parameter $C_{1\epsilon}$ on predicted mean temperature profiles at several axial locations in radial direction and along the centerline (EDC model version: 'EDC2005').

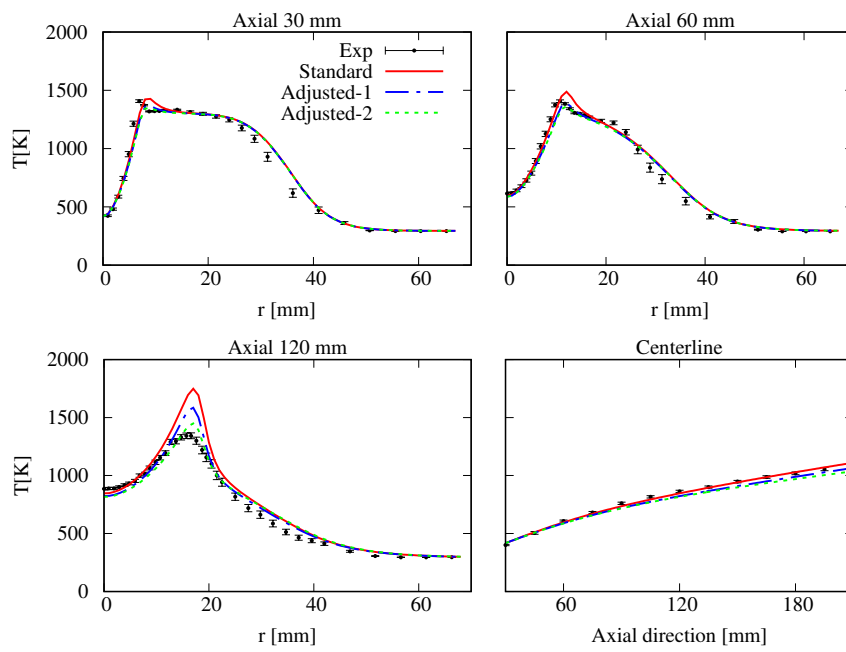


Figure 5: Effects of the adjusted EDC constants on predicted mean temperature profiles at several axial locations in radial direction and along the centerline.

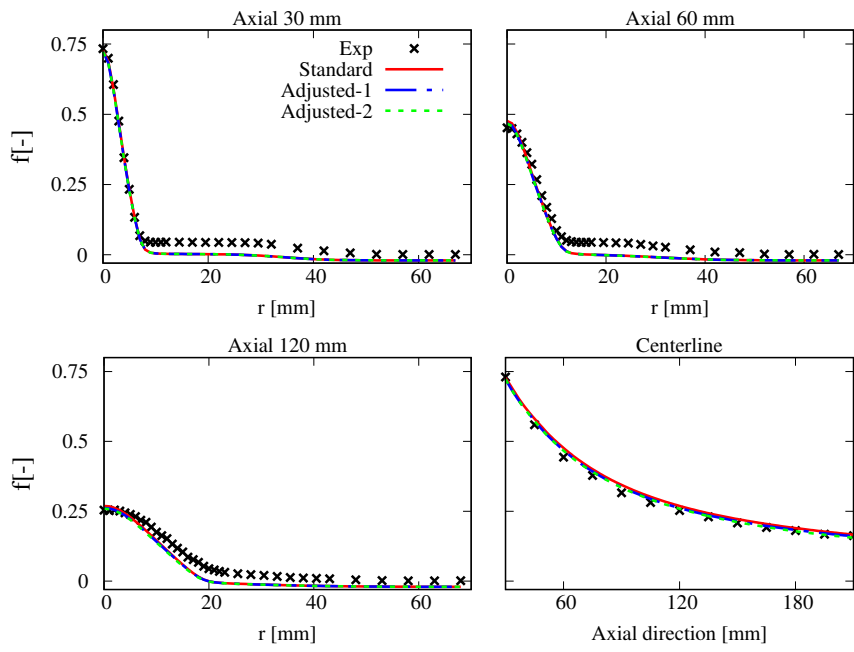


Figure 6: Effects of the adjusted EDC constants on mixture fraction profiles at several axial locations in radial direction and along the centerline.

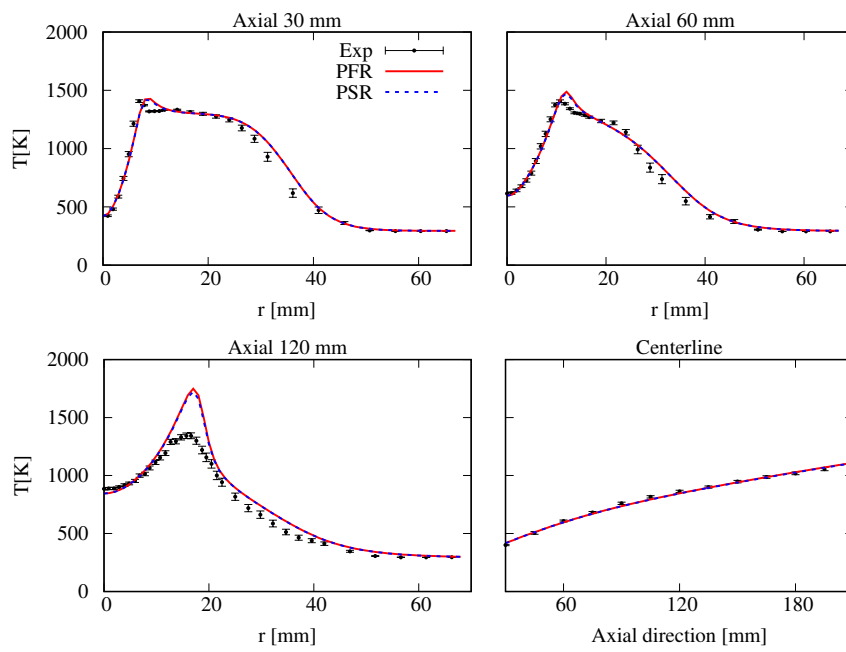


Figure 7: Effects of the canonical reactor (PFR vs. PSR) on predicted mean temperature profiles at several axial locations in radial direction and along the centerline.

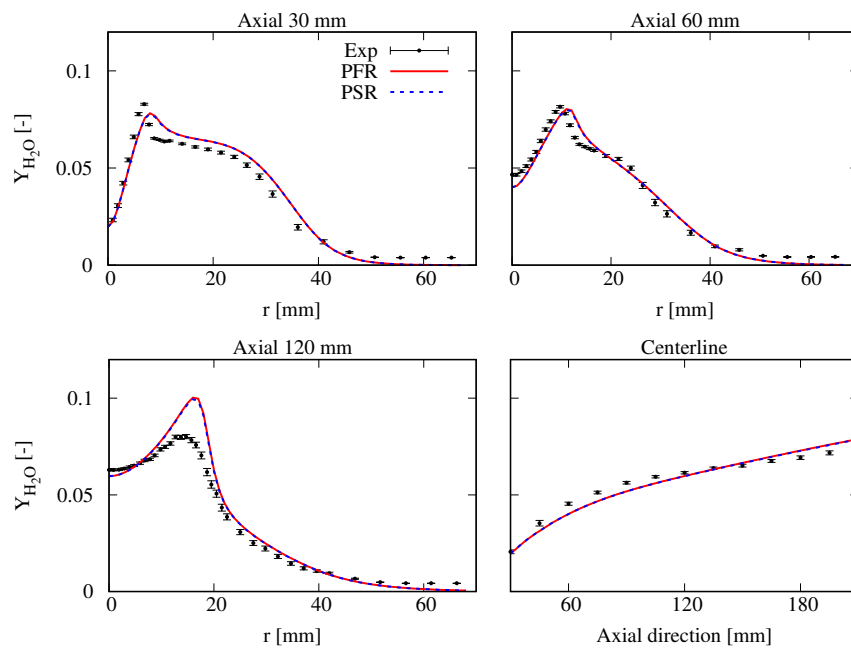


Figure 8: Effects of the canonical reactor (PFR vs. PSR) on predicted mean H₂O mass fraction profiles at several axial locations in radial direction and along the centerline.

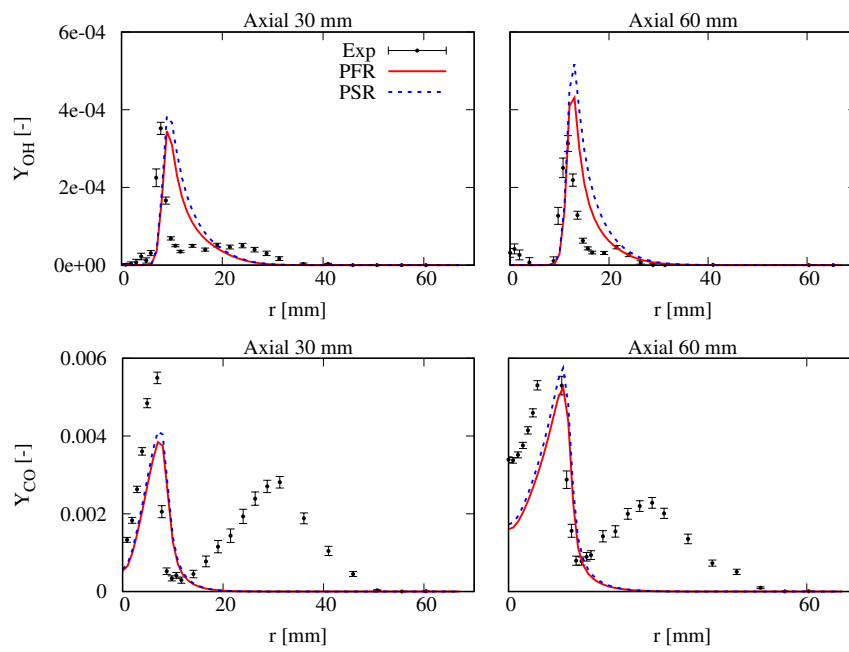


Figure 9: Effects of the canonical reactor (PFR vs. PSR) on predicted mean OH and CO mass fraction profiles at 30 mm and 60 mm axial locations in radial direction.

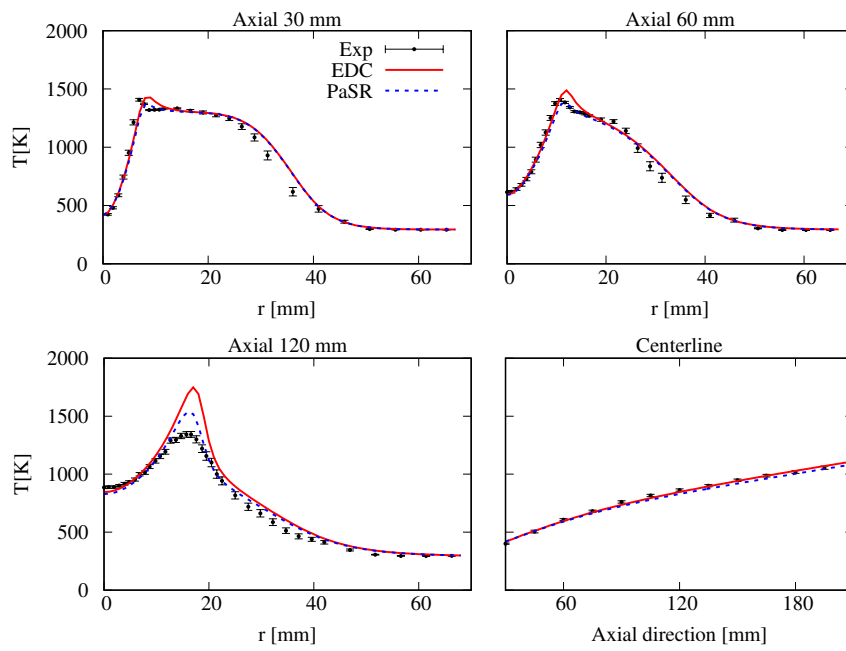


Figure 10: Comparison between the experimental and numerical mean temperature profiles at several axial locations in radial direction and along the centerline. Combustion models: EDC and PaSR.

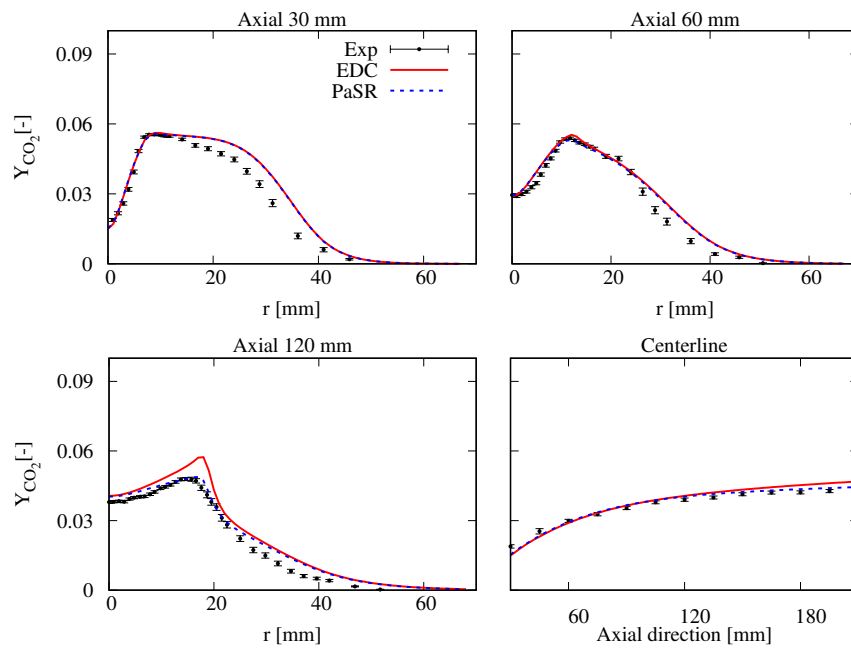


Figure 11: Comparison between the experimental and numerical mean CO_2 mass fraction profiles at several axial locations in radial direction and along the centerline. Combustion models: EDC and PaSR.

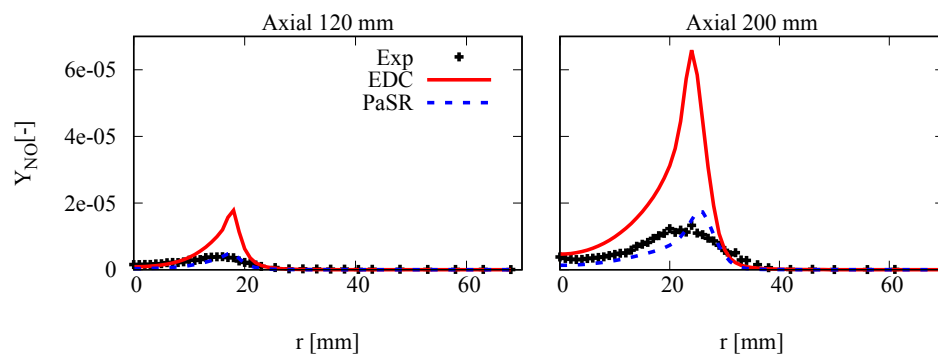


Figure 12: Comparison of the mean NO mass fraction radial profiles using the EDC and PaSR models at 120 mm and 200 mm axial locations.

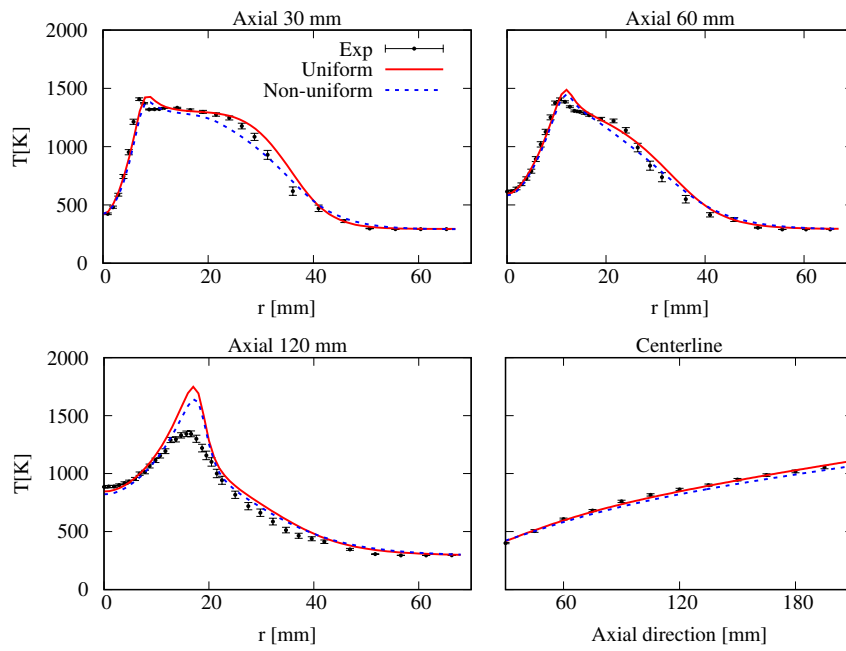


Figure 13: Comparison of the mean temperature profiles from the cases with uniform boundary conditions and non-uniform boundary conditions at several axial locations in radial direction and along the centerline.

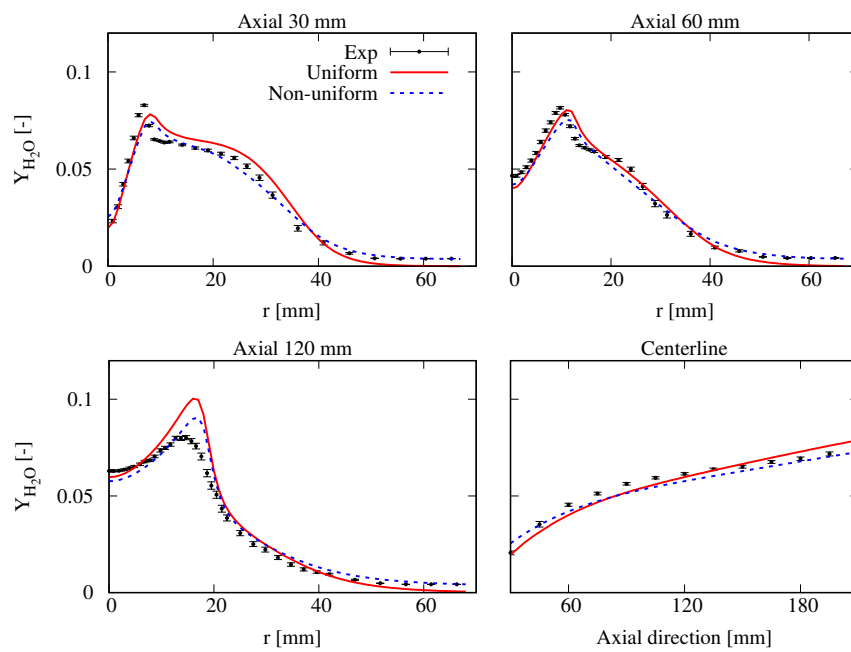


Figure 14: Comparison of the mean H_2O mass fraction profiles from the cases with uniform boundary conditions and non-uniform boundary conditions at several axial locations in radial direction and along the centerline.

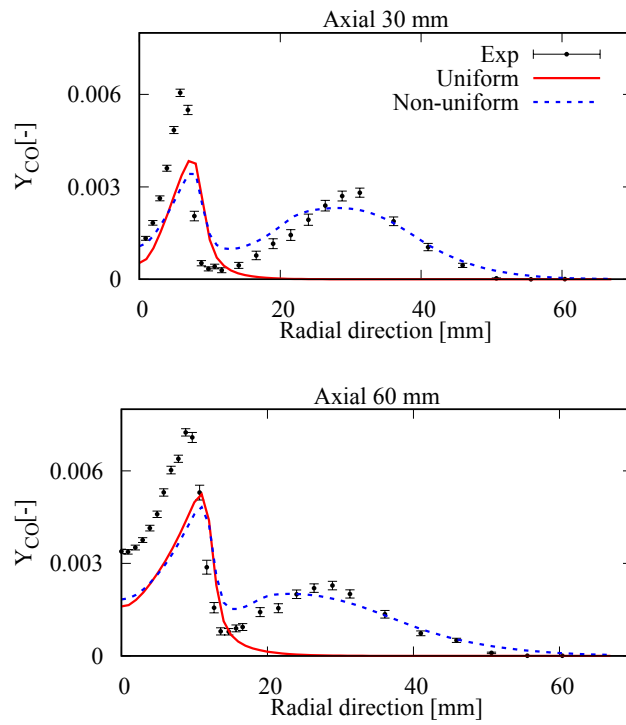


Figure 15: Comparison of the mean CO mass fraction profiles from the cases with uniform boundary conditions and non-uniform boundary conditions at 30 *mm* and 60 *mm* axial locations in radial direction.

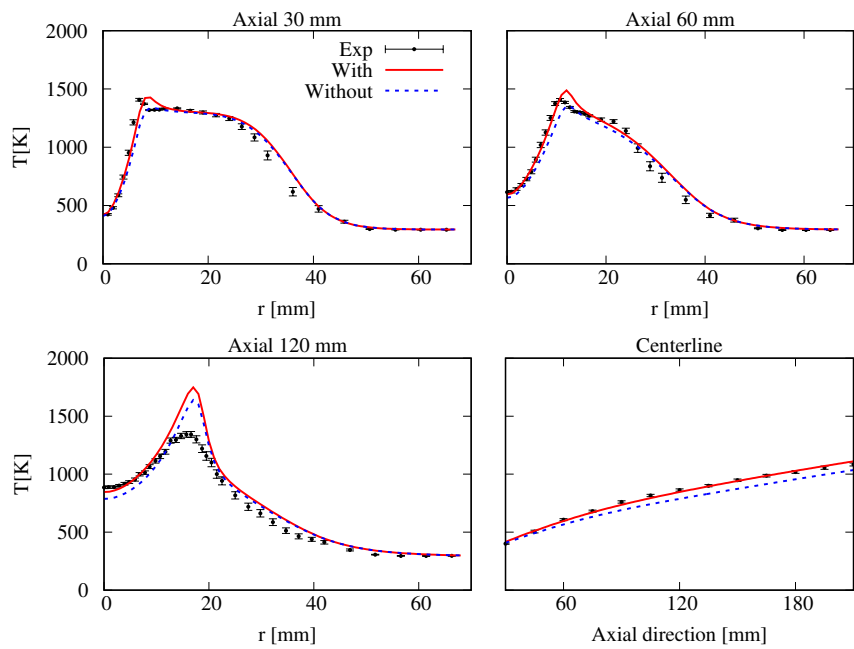


Figure 16: Comparison of the mean temperature profiles from the cases with and without multi-component molecular diffusion at several axial locations in radial direction and along the centerline.

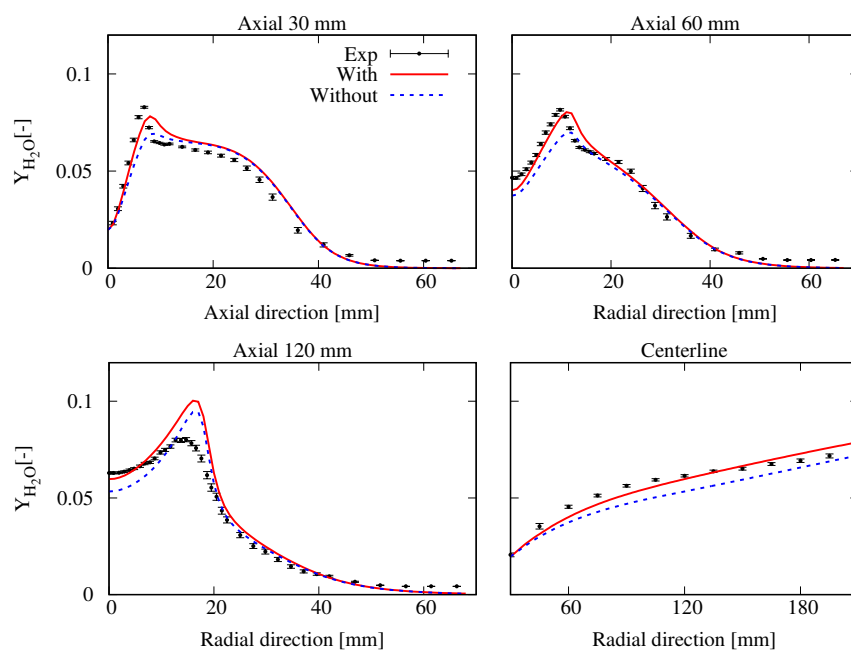


Figure 17: Comparison of the mean H_2O mass fraction profiles from the cases with and without multi-component molecular diffusion at several axial locations in radial direction and along the centerline.

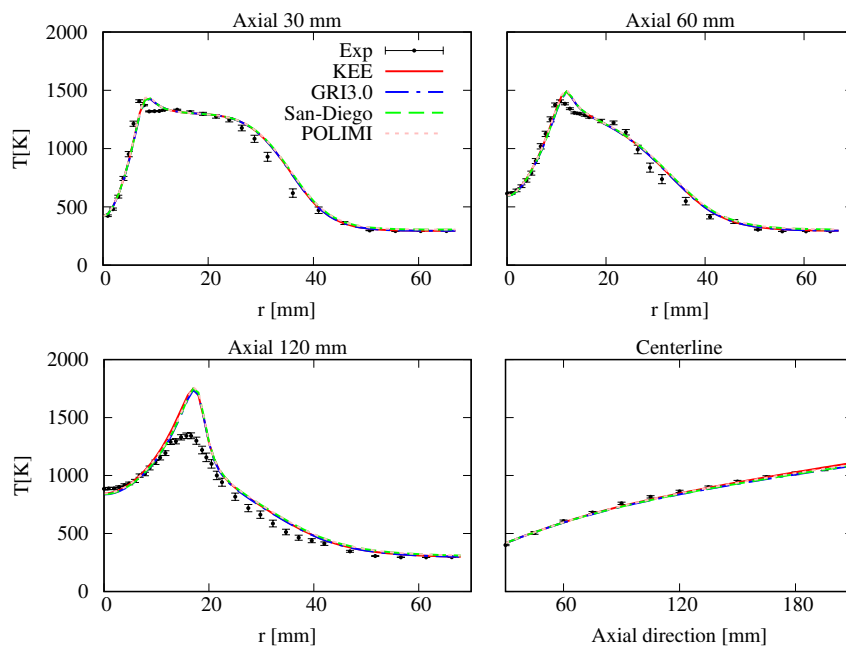


Figure 18: Comparison of the mean temperature profiles from the cases with different kinetic mechanisms at several axial locations in radial direction and along the centerline.

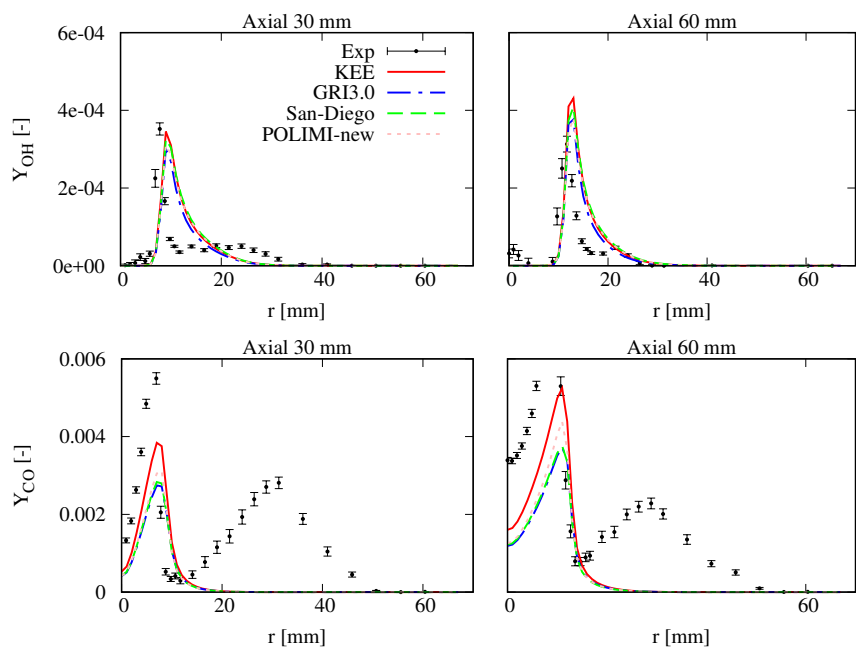


Figure 19: Comparison of the OH and CO mass fraction profiles from the cases with different kinetic mechanisms at 30 mm and 60 mm axial locations in radial direction.

Table 1: Physical properties of the jet

Profiles	Central jet	Annulus	Tunnel
Velocity	58.74 <i>m/s</i>	3.2 <i>m/s</i>	3.3 <i>m/s</i>
Temperature	294 <i>K</i>	1300 <i>K</i>	294 <i>K</i>

Table 2: Limitations of fine structure fraction

EDC version	time scale ratio	γ_λ limit
'EDC1981'	$\frac{\gamma_\lambda^3}{1-\gamma_\lambda^3}$	0.7937
'EDC1996'	$\frac{\gamma_\lambda^2}{1-\gamma_\lambda^3}$	0.7549
'EDC2005'	$\frac{\gamma_\lambda^2}{1-\gamma_\lambda^2}$	0.7071

Table 3: Grid Convergence Index (GCI) for different grids

Mesh resolution	coarse	medium	fine	superfine
Number of cells	15900	34830	79110	179186
GCI (%)	0.93	1.52	1.87	1.92

Table 4: Discretization schemes

Field	Discretization scheme
Velocity (U)	Total Variance Diminishing (TVD)
Pressure (p)	Total Variance Diminishing (TVD)
Species mass fraction (Y)	bounded ([0,1]) TVD

Table 5: Uniform boundary condition values for the JHC burner

Boundaries	Inlet fuel	Inlet co-flow	Inlet air
Temperature (K)	305	1300	294
Velocity (m/s)	58.74	3.2	3.3
CH4 mass fraction (-)	0.888	0	0
H2 mass fraction (-)	0.112	0	0
O2 mass fraction (-)	0	0.03	0.232

Table 6: Numerical Settings of the Reference Case

Turbulent Schmidt Number	0.7
Turbulent Prandtl Number	0.85
$k - \epsilon$ model constant $C_{1\epsilon}$	1.60
Combustion Model	Eddy Dissipation Concept
EDC model version	'EDC1996'
EDC model constant	standard
Canonical reactor	PFR
Kinetic mechanism	KEE
Boundary conditions	uniform
Radiation model	none
Multi-component molecular diffusion	on